

Finite element discretization and iterative solution techniques for multiphase flows in gas-liquid reactors

D. Kuzmin* and S. Turek

*Institute of Applied Mathematics, University of Dortmund
Vogelpothsweg 87, D-44227, Dortmund, Germany*

Abstract

A mathematical model for gas-liquid flows subject to mass transfer and chemical reactions is presented. It is shown that bubble-induced buoyancy resembles natural convection and can readily be incorporated into an incompressible flow solver by using an analog of the Boussinesq approximation. Extra transport equations with nonlinear source terms are introduced to describe the evolution of scalar quantities. A segregated algorithm is proposed for the numerical treatment of the resulting PDE system. The Navier-Stokes equations are solved by a projection-like method based on the Pressure Schur Complement approach. Novel high-resolution finite element schemes of FCT and TVD type are employed for the discretization of unstable convective terms. Numerical results for a number of prototypical gas-liquid reactor configurations illustrate the performance of the developed simulation tools.

Key Words: computational fluid dynamics; bubble columns; airlift loop reactors
finite elements; incompressible flow solvers; high-resolution schemes

AMS Subject Classification: 65F10, 65M60, 76T10

1 Introduction

Bubble columns and airlift loop reactors are widely used in industry as contacting devices in which gaseous and liquid species are brought together to engage in chemical reactions. The liquid supplied continuously or in a batch mode is agitated by bubbles fed at the bottom of the reactor. As the bubbles rise, the gaseous component is gradually absorbed into the bulk liquid where it may react with other species. The geometric simplicity of bubble columns makes them rather easy to build, operate and maintain. At the same time, the prevailing flow patterns are very complex and unpredictable, which represents a major bottleneck for the design of industrial units. In airlift loop reactors, internal parts are installed in order to enforce a stable circulation of liquid characterized by the presence of pronounced *riser* and *downcomer* zones. Shape optimization appears to be a promising way to improve the reactor performance by adjusting the geometry of internals.

In this paper, we touch upon the mathematical modeling of gas-liquid flows and propose a numerical algorithm based on the finite element method. A hierarchy of successively refined unstructured meshes is used to deal with complex domains. The velocity-pressure coupling via the incompressibility constraint is imposed in the framework of the Multilevel

*Correspondence to: kuzmin@math.uni-dortmund.de

Pressure Schur Complement formulation originally developed for single-phase flows [29]. The instability of convective terms poses a hazard to the positivity of gas holdup and concentrations. Standard remedies like upwinding degrade the accuracy of the numerical solution and produce unacceptable results. The only way to obtain a sharp resolution of steep fronts without generating wiggles is to use a nonlinear combination of high- and low-order methods. The main contribution of this paper is a truly multidimensional generalization of high-resolution TVD schemes to finite element discretizations on arbitrary meshes. Alternatively, convective terms can be handled by the implicit FEM-FCT methodology which is presented in detail elsewhere [11], [13], [14]. Furthermore, we discuss some other algorithmic aspects relevant for simulation of gas-liquid flows. Numerical examples are presented to give a flavor of feasible applications. However, a detailed analysis of the model and of the obtained results is beyond the scope of this paper.

2 Mathematical model

Detailed hydrodynamic models for dispersed two-phase flow can be classified into those of Euler-Euler and Euler-Lagrange type. The former approach implies that both phases are treated as space-sharing interpenetrating continua. The macroscopic conservation laws can be postulated using some heuristic arguments or derived mathematically by applying a suitable averaging procedure to the associated single-phase continuity and momentum equations [4], [5]. In the Euler-Lagrange formulation, only the liquid phase is considered to be continuous, while individual bubbles or bubble clusters are tracked in a Lagrangian way [15], [25]. The most detailed treatment of gas-liquid flow is provided by direct numerical simulation (DNS), which amounts to solving a formidable free boundary problem for the deformation of all bubbles and interactions between them. At present, this is feasible only for a very limited number of bubbles. Nevertheless, DNS contributes to the understanding of processes taking place at the microscopic level and constitutes a valuable tool for the derivation of input parameters and correlations for less sophisticated CFD models.

In this paper, we subscribe to the Euler-Euler approach whereby the computational cost is largely independent of the number of bubbles present in the flow field. The instantaneous distribution of phases in the reactor is determined by the local gas holdup $\alpha_G = \epsilon$. The volume fraction of liquid equals $\alpha_L = 1 - \epsilon$. The macroscopic continuity equations

$$\frac{\partial \tilde{\rho}_G}{\partial t} + \nabla \cdot (\tilde{\rho}_G \mathbf{u}_G) = -m_{\text{int}}, \quad \tilde{\rho}_G = \alpha_G \rho_G, \quad (1)$$

$$\frac{\partial \tilde{\rho}_L}{\partial t} + \nabla \cdot (\tilde{\rho}_L \mathbf{u}_L) = m_{\text{int}}, \quad \tilde{\rho}_L = \alpha_L \rho_L \quad (2)$$

are coupled by the mass transfer term m_{int} which models the absorption of gas into the liquid. Here and below the tilde denotes multiplication by the volume fraction of the respective phase. The macroscopic momentum equations read

$$\tilde{\rho}_G \left[\frac{\partial \mathbf{u}_G}{\partial t} + \mathbf{u}_G \cdot \nabla \mathbf{u}_G \right] = \alpha_G \nabla \cdot \mathcal{S}_G + \tilde{\rho}_G \mathbf{g} + \mathbf{f}_{\text{int}}, \quad (3)$$

$$\tilde{\rho}_L \left[\frac{\partial \mathbf{u}_L}{\partial t} + \mathbf{u}_L \cdot \nabla \mathbf{u}_L \right] = \alpha_L \nabla \cdot \mathcal{S}_L + \tilde{\rho}_L \mathbf{g} - \mathbf{f}_{\text{int}}, \quad (4)$$

where \mathcal{S} refers to the stress tensor and the coupling term \mathbf{f}_{int} in both right-hand sides is responsible for the momentum exchange at the gas-liquid interface.

The above system of equations is known as the *two-fluid model*, which is widespread in the CFD community. It provides a general description of the two-phase flow but is practically worthless as long as the terms m_{int} , \mathbf{f}_{int} , \mathcal{S}_G , \mathcal{S}_L are left unspecified. The derivation of appropriate closure relations is a challenging task due to various interactions between the two phases. In what follows, we present constitutive equations suitable for buoyancy-driven bubbly flows with mass transfer and chemical reaction.

2.1 Interphase mass transfer

The mass transfer rate is proportional to the difference between the concentration c_A of the dissolved gas and an equilibrium concentration c_A^* . The latter is related to the local pressure p via Henry's law $p = Hc_A^*$, where H is an empirical coefficient depending on the solubility of gas. The total flux of gas into the liquid is given by

$$m_{\text{int}} = k_L a_S (c_A^* - c_A) \eta, \quad (5)$$

where a_S stands for the specific interfacial area, η denotes the molecular weight of gaseous species and k_L is the liquid-side mass transfer coefficient. As a rule, the resistance to mass transfer on the gas side can be neglected.

Chemical reactions in the liquid phase can substantially accelerate the absorption process by increasing the concentration gradient. The concomitant increase in the gas flux is taken into account by applying an enhancement factor E to the physical mass transfer coefficient:

$$k_L = Ek_L^0, \quad (6)$$

where k_L^0 is a function of the Sherwood number Sh which varies with the local Peclet number Pe . For a first-order irreversible reaction, the standard film theory yields [22]

$$E = Ha \coth Ha, \quad (7)$$

where Ha is the Hatta number. For vanishing Ha , the hyperbolic tangent tends to zero, so that the above equation should be replaced by the series

$$E = 1 + \frac{1}{3}Ha^2 - \frac{1}{45}Ha^4 + \frac{2}{945}Ha^6 - \frac{1}{4725}Ha^8 + \dots \quad (8)$$

The enhancement factor for second-order reactions $A + \nu_B B \rightarrow \nu_P P$ can be derived analytically only in a few limiting cases, e.g. for an instantaneous irreversible reaction:

$$E_i = 1 + \frac{d_B c_B}{\nu_B d_A c_A^*}, \quad (9)$$

d_A and d_B being the molecular diffusion coefficients. For slow and intermediate reactions, equations of the film model have to be solved approximately. A widely used correlation of numerical results was introduced by Van Krevelen and Hoftijzer [31]:

$$E = M \coth M, \quad M = Ha \sqrt{\frac{E_i - E}{E_i - 1}}. \quad (10)$$

Note that this equation is nonlinear and has to be solved iteratively or approximated by a simpler formula due to Wellek *et al.* [32]

$$\frac{1}{(E-1)^{1.35}} = \frac{1}{(E_i-1)^{1.35}} + \frac{1}{(E_1-1)^{1.35}}, \quad E_1 = Ha \coth Ha. \quad (11)$$

Recall that the mass transfer term (5) contains the interfacial area a_S which still is to be defined. This key variable depends on the number and size of bubbles which may vary in space and time. If there is no coalescence and breakup of bubbles, their number density is conserved and satisfies the continuity equation

$$\frac{\partial n}{\partial t} + \nabla \cdot (n \mathbf{u}_G) = 0. \quad (12)$$

Let us assume that the gas-liquid mixture is locally monodisperse, i.e. the bubbles are spherical with an average radius r . As long as n represents the number of bubbles per unit volume, multiplying it by the volume of a single bubble yields the local gas holdup $\epsilon = \frac{4}{3}\pi r^3 n$. Hence, the specific interfacial area $a_S = 4\pi r^2 n$ is given by

$$a_S = (4\pi n)^{1/3} (3\epsilon)^{2/3}, \quad \text{where } \epsilon = \frac{\tilde{\rho}_G}{\rho_G} = \tilde{\rho}_G \frac{RT}{p\eta}. \quad (13)$$

Here the physical density ρ_G is evaluated using the ideal gas law. The effective density $\tilde{\rho}_G$ is computed from the continuity equation (1) for the gas phase.

2.2 Chemical reactions

The concentrations of all species dissolved in the liquid phase are described by a system of scalar transport equations with source and/or sink terms due to mass transfer and chemical reactions. For homogeneous reactions of second order it reads

$$\frac{\partial \tilde{c}_A}{\partial t} + \nabla \cdot (\tilde{c}_A \mathbf{u}_L - \tilde{d}_A \nabla c_A) = \frac{m_{\text{int}}}{\eta} - \tilde{k}_2 c_A c_B, \quad (14)$$

$$\frac{\partial \tilde{c}_B}{\partial t} + \nabla \cdot (\tilde{c}_B \mathbf{u}_L - \tilde{d}_B \nabla c_B) = -\nu_B \tilde{k}_2 c_A c_B, \quad (15)$$

$$\frac{\partial \tilde{c}_P}{\partial t} + \nabla \cdot (\tilde{c}_P \mathbf{u}_L - \tilde{d}_P \nabla c_P) = \nu_P \tilde{k}_2 c_A c_B, \quad (16)$$

where the subscript A denotes the dissolved gas, B the component it reacts with and P the resulting product. The effective diffusion coefficients $\tilde{d}_A, \tilde{d}_B, \tilde{d}_P$ may involve contributions of the turbulent dispersion in the liquid phase.

If the reactant B is present in excess, its virtually constant concentration can be built into the reaction rate $k_1 = k_2 c_B$, and the reaction is said to be a pseudo-first-order one. In this case, the system of mass balances shrinks to

$$\frac{\partial \tilde{c}_A}{\partial t} + \nabla \cdot (\tilde{c}_A \mathbf{u}_L - \tilde{d}_A \nabla c_A) = \frac{m_{\text{int}}}{\eta} - \tilde{k}_1 c_A, \quad (17)$$

$$\frac{\partial \tilde{c}_P}{\partial t} + \nabla \cdot (\tilde{c}_P \mathbf{u}_L - \tilde{d}_P \nabla c_P) = \nu_P \tilde{k}_1 c_A, \quad (18)$$

and the enhancement factor is defined by equation (7) rather than (10) or (11). In any event, the concentration fields have little or no effect on the liquid velocity, so the above transport equations are essentially decoupled from the rest of the model.

2.3 Closure of the momentum equations

Both phases are considered to be Newtonian fluids sharing the same pressure field. Hence, the stress tensor for either phase can be represented as

$$\mathcal{S}(\mathbf{u}) = -p\mathcal{I} + \mu_{\text{eff}}\mathcal{D}(\mathbf{u}), \quad (19)$$

where the pressure p and the deformation rate tensor \mathcal{D} are defined by

$$p = \rho_G \frac{R}{\eta} T, \quad \mathcal{D}(\mathbf{u}) = \frac{1}{2}[\nabla\mathbf{u} + \nabla\mathbf{u}^T].$$

For simplicity, the effective viscosity μ_{eff} is assumed to be constant. In general, it consists of the laminar viscosity μ depending solely on the physical properties of the fluid and the turbulent eddy viscosity μ_T modeling the effect of microscopic velocity fluctuations which are eliminated during the averaging process. The standard $k - \epsilon$ turbulence model seems to perform reasonably well [2], [24] and can be extended to allow for the bubble-induced turbulence [9], [19]. Nevertheless, turbulence modeling for two-phase flows remains an open question and no reliable model is available to date.

The coupling term \mathbf{f}_{int} in the balance equations (3) and (4) represents the interphase momentum transfer due to forces exerted by the liquid phase on the rising bubbles. In spite of the ongoing controversy in the literature, it is generally accepted that \mathbf{f}_{int} involves contributions from the drag force, the virtual mass force and the lift force [5]:

$$\mathbf{f}_{\text{int}} = \mathbf{f}_D + \mathbf{f}_{VM} + \mathbf{f}_L. \quad (20)$$

By far the most important constituent is the drag force \mathbf{f}_D experienced by a bubble as it moves steadily in the surrounding liquid. The ensuing interphase friction is given by

$$\mathbf{f}_D = -\epsilon C_D \frac{3}{8} \frac{\rho_L}{r} |\mathbf{u}_G - \mathbf{u}_L| (\mathbf{u}_G - \mathbf{u}_L), \quad (21)$$

where C_D is a dimensionless drag coefficient which can be assessed by measuring the terminal rise velocity of a single bubble. Numerous empirical correlations are available for C_D as a function of the Reynolds number. Note that the drag force is proportional to the relative velocity so that the bubbles slow down whereas the liquid gains momentum.

The ‘added mass’ of liquid entrained in the wake of accelerating bubbles results in a virtual mass force of the form

$$\mathbf{f}_{VM} = -\epsilon C_{VM} \rho_L \left(\frac{d\mathbf{u}_G}{dt} - \frac{d\mathbf{u}_L}{dt} \right). \quad (22)$$

Depending on the properties of the gas-liquid mixture, the virtual mass coefficient C_{VM} may deviate appreciably from the default value $C_{VM} = 0.5$ valid for spherical particles under some idealistic assumptions.

Additional forces transverse to the direction of motion are typically represented by

$$\mathbf{f}_L = -\epsilon C_L \rho_L (\mathbf{u}_G - \mathbf{u}_L) \times (\nabla \times \mathbf{u}_L), \quad (23)$$

where the lift coefficient C_L equals 0.25 for dilute flows of spheres.

2.4 Algebraic slip relation

The implications of the three contributions to the interphase force were analyzed in detail by Sokolichin and Eigenberger [23]. They demonstrated that the influence of the virtual mass force \mathbf{f}_{VM} on the bubble motion can be neglected. At the same time, they found the lift force to be rather significant but questioned its existence in the form (23) which was originally derived for solid particles. In the literature, \mathbf{f}_L is often misused for fitting the results to experimental data. In some publications even the sign of the lift coefficient is reversed. Sokolichin and Eigenberger condemned this practice and argued that the lift force should be omitted as long as its origins, form and magnitude are unclear.

The interphase momentum transfer is dominated by the drag force \mathbf{f}_D and the above arguments indicate that it is the only one which needs to be taken into account. Moreover, the density of gas is much smaller than that of liquid, so that the inertia and gravity terms in the gas phase momentum balance (3) can be neglected [23]. Assuming the gas phase to be inviscid, we insert the stress tensor $\mathcal{S}_G = p\mathcal{I}$ and obtain the equilibrium relation

$$0 = -\epsilon\nabla p + \mathbf{f}_D, \quad (24)$$

which can be used to compute the relative bubble velocity \mathbf{u}_{slip} . To this end, it is expedient to linearize the drag force as proposed by Schwarz and Turner [21]:

$$\mathbf{f}_D = -\epsilon C_D \frac{3\rho_L}{8} \frac{1}{r} |\mathbf{u}_{\text{slip}}| \mathbf{u}_{\text{slip}} \approx -\epsilon C_W \mathbf{u}_{\text{slip}} \quad \Rightarrow \quad \mathbf{u}_{\text{slip}} = -\frac{\nabla p}{C_W}. \quad (25)$$

Unlike the standard drag coefficient C_D , the linearization parameter C_W is a dimensional quantity. It is commonly assigned the constant value $5 \cdot 10^4 \frac{\text{kg}}{\text{m}^3 \text{s}}$ which corresponds to the bubble rise velocity of approximately 20 cm/s.

The above model simplifications make it possible to replace the gas phase momentum balance by the algebraic slip relation

$$\mathbf{u}_G = \mathbf{u}_L + \mathbf{u}_{\text{slip}} + \mathbf{u}_{\text{drift}}, \quad (26)$$

where the drift velocity $\mathbf{u}_{\text{drift}}$ was introduced to model the transport of bubbles by turbulent eddies. The net flux of gas due to turbulent dispersion is proportional to the gradient of the number density and directed opposite to it. The corresponding drift velocity reads

$$\mathbf{u}_{\text{drift}} = -d_G \frac{\nabla n}{n}. \quad (27)$$

In general, the bubble path dispersion coefficient d_G depends on the eddy viscosity μ_T and on the turbulent Schmidt number [23].

If the velocity \mathbf{u}_G is computed from the slip relation (26) making use of (27), the gas phase continuity equations (1) and (12) can be rewritten the form

$$\frac{\partial \tilde{\rho}_G}{\partial t} + \nabla \cdot (\tilde{\rho}_G (\mathbf{u}_L + \mathbf{u}_{\text{slip}}) - d_G \nabla \tilde{\rho}_G) = -m_{\text{int}} \quad (28)$$

and

$$\frac{\partial n}{\partial t} + \nabla \cdot (n (\mathbf{u}_L + \mathbf{u}_{\text{slip}}) - d_G \nabla n) = 0, \quad (29)$$

respectively. Strictly speaking, the diffusive term in (28) is valid only for a constant bubble mass but this form can be justified if one substitutes the drift velocity after decoupling the transport and mass transfer (see the description of operator splitting tools below).

2.5 Drift-flux model

The two-fluid model (1)–(4) is not the only way to describe dispersed two-phase flows using a fully continuous representation. Alternatively, the gas-liquid mixture can be considered as a single fluid whose effective density and momentum are defined by

$$\rho = \tilde{\rho}_L + \tilde{\rho}_G, \quad \rho \mathbf{u} = \tilde{\rho}_L \mathbf{u}_L + \tilde{\rho}_G \mathbf{u}_G. \quad (30)$$

The weakly compressible Navier-Stokes equations for these quantities constitute the so-called drift-flux model. As soon as the mixture velocity \mathbf{u} is available, the velocities of both phases can be recovered using the algebraic slip relation (26).

For bubbly flows, the two-fluid model and the drift-flux model are essentially equivalent [23]. Indeed, the sum of phasic continuity equations (1) and (2) yields

$$\frac{\partial \rho}{\partial t} + \nabla \cdot (\rho \mathbf{u}) = 0. \quad (31)$$

Furthermore, if the simplified gas phase momentum balance (24) is added to equation (4) with the stress tensor \mathcal{S}_L given by (19), the interphase force term vanishes and we obtain

$$\tilde{\rho}_L \left[\frac{\partial \mathbf{u}_L}{\partial t} + \mathbf{u}_L \cdot \nabla \mathbf{u}_L \right] = -\nabla p + \nabla \cdot (\tilde{\mu}_{\text{eff}} \mathcal{D}(\mathbf{u}_L)) + \tilde{\rho}_L \mathbf{g}. \quad (32)$$

Recall that the gas density is very small as compared to that of liquid. Therefore, its contribution to the mixture density and momentum can be neglected:

$$\rho \approx \tilde{\rho}_L, \quad \mathbf{u} \approx \mathbf{u}_L. \quad (33)$$

Under these assumptions, equation (32) reduces to the momentum balance for the mixture.

2.6 Boussinesq approximation

The effective density $\tilde{\rho}_L = (1 - \epsilon)\rho_L$ depends on the local gas holdup, which leads to liquid circulation due to the buoyancy in aerated regions. Similar processes occur in single-phase flows in the presence of temperature gradients. Following Sokolichin and Eigenberger [23], we use an analog of the Boussinesq approximation for natural convection problems and retain the variable density only in the gravity term of equation (32) dropping the tilde elsewhere. After these modifications, we recover the incompressible Navier-Stokes equations with an extra buoyancy term proportional to the gas holdup:

$$\begin{aligned} \frac{\partial \mathbf{u}_L}{\partial t} + \mathbf{u}_L \cdot \nabla \mathbf{u}_L &= -\nabla p_* + \nu_{\text{eff}} \Delta \mathbf{u}_L - \epsilon \mathbf{g}, \\ \nabla \cdot \mathbf{u}_L &= 0, \quad p_* = \frac{p - p_{\text{atm}}}{\rho_L} + \mathbf{g} \cdot \mathbf{x} - gh. \end{aligned} \quad (34)$$

At high gas throughputs it is advisable to relax the Boussinesq approximation in the momentum equation and solve it in its original form (32). As far as the continuity equation is concerned, the constant density assumption can be retained. This model simplification is particularly advantageous from the computational viewpoint, since it eliminates the need for dealing with the evolution of the free surface on top of the reactor [23].

2.7 Summary of equations

As a bottomline, let us collect the equations to be solved. Our simplified Euler-Euler model of drift-flux type consists of the following subproblems:

- Navier-Stokes/‘Boussinesq’ equations

$$\begin{aligned} \frac{\partial \mathbf{u}_L}{\partial t} + \mathbf{u}_L \cdot \nabla \mathbf{u}_L &= -\nabla p_* + \nu_{\text{eff}} \Delta \mathbf{u} - \epsilon \mathbf{g}, \\ \nabla \cdot \mathbf{u}_L &= 0. \end{aligned} \quad (35)$$

- Continuity equations for the gas phase

$$\frac{\partial \tilde{\rho}_G}{\partial t} + \nabla \cdot (\tilde{\rho}_G(\mathbf{u}_L + \mathbf{u}_{\text{slip}}) - d_G \nabla \tilde{\rho}_G) = -m_{\text{int}}, \quad (36)$$

$$\frac{\partial n}{\partial t} + \nabla \cdot (n(\mathbf{u}_L + \mathbf{u}_{\text{slip}}) - d_G \nabla n) = 0. \quad (37)$$

- Transport equations for the liquid phase

$$\frac{\partial \tilde{c}_A}{\partial t} + \nabla \cdot (\tilde{c}_A \mathbf{u}_L - \tilde{d}_A \nabla c_A) = \frac{m_{\text{int}}}{\eta} - \tilde{k}_2 c_A c_B, \quad (38)$$

$$\frac{\partial \tilde{c}_B}{\partial t} + \nabla \cdot (\tilde{c}_B \mathbf{u}_L - \tilde{d}_B \nabla c_B) = -\nu_B \tilde{k}_2 c_A c_B, \quad (39)$$

$$\frac{\partial \tilde{c}_P}{\partial t} + \nabla \cdot (\tilde{c}_P \mathbf{u}_L - \tilde{d}_P \nabla c_P) = \nu_P \tilde{k}_2 c_A c_B. \quad (40)$$

These partial differential equations are supplemented by the algebraic closure relations

$$\begin{aligned} \mathbf{u}_{\text{slip}} &= -\frac{\nabla p}{C_W}, \quad m_{\text{int}} = Ek_L^0 a_S \left(\frac{p}{H} - c_A \right) \eta, \\ \epsilon &= \frac{\tilde{\rho}_G R T}{p \eta}, \quad a_S = (4\pi n)^{1/3} (3\epsilon)^{2/3}, \quad \nu_{\text{eff}} = \text{const.} \end{aligned}$$

The problem statement is to be completed by specifying appropriate initial and boundary conditions which depend on the particular application.

3 Numerical algorithm

The main features of the numerical algorithm are summarized below. The discretization in space is performed by an unstructured grid finite element method in order to provide an accurate treatment of non-Cartesian geometries with internal obstacles. The incompressible Navier-Stokes equations call for the use of an LBB-stable finite element pair. A suitable candidate is the nonconforming Rannacher-Turek element (rotated multilinear velocity, piecewise-constant pressure) [20]. Standard multilinear elements are employed for other variables. The manually generated coarse mesh is successively refined to produce hierarchical data structures for the multigrid solver [27], [28].

The coupled subproblems are solved one at a time within a block-iterative loop of Gauß-Seidel type. A two-way coupling is implemented only for the hydrodynamic part $(\mathbf{u}_L, p, \epsilon)$. We solve the Navier-Stokes equations using the gas holdup from the last outer iteration, then update the gas holdup and repeat this procedure until the residual of the momentum equation or the relative changes of the gas holdup distribution are small enough. The resulting velocity field is substituted into the transport equations (37)–(40) and remains fixed until the end of the time step.

Operator splitting is employed to separate convection-diffusion and absorption-reaction processes. First, all scalar quantities are transported without taking the sources/sinks into account. The homogeneous equations (41)–(44) are decoupled and can be processed in parallel. The updated concentration fields serve as initial data for an ODE system which describes the accumulation and consumption of species. Equations (45)–(48) are nonlinear and strongly coupled but the nodal ODE systems are independent of one another.

Step 1: convection-diffusion

$$\frac{\partial \tilde{\rho}_G}{\partial t} + \nabla \cdot (\tilde{\rho}_G(\mathbf{u}_L + \mathbf{u}_{\text{slip}}) - d_G \nabla \tilde{\rho}_G) = 0, \quad (41)$$

$$\frac{\partial \tilde{c}_A}{\partial t} + \nabla \cdot (\tilde{c}_A \mathbf{u}_L - \tilde{d}_A \nabla c_A) = 0, \quad (42)$$

$$\frac{\partial \tilde{c}_B}{\partial t} + \nabla \cdot (\tilde{c}_B \mathbf{u}_L - \tilde{d}_B \nabla c_B) = 0, \quad (43)$$

$$\frac{\partial \tilde{c}_P}{\partial t} + \nabla \cdot (\tilde{c}_P \mathbf{u}_L - \tilde{d}_P \nabla c_P) = 0. \quad (44)$$

Step 2: absorption-reaction

$$\frac{d \tilde{\rho}_G}{dt} = -m_{\text{int}}, \quad (45)$$

$$\frac{d \tilde{c}_A}{dt} = \frac{m_{\text{int}}}{\eta} - \tilde{k}_2 c_A c_B, \quad (46)$$

$$\frac{d \tilde{c}_B}{dt} = -\nu_B \tilde{k}_2 c_A c_B, \quad (47)$$

$$\frac{d \tilde{c}_P}{dt} = \nu_P \tilde{k}_2 c_A c_B. \quad (48)$$

Note that operator splitting is applied locally in time, i.e. within each time step. The solution is integrated in time from t_n to $t_{n+1} = t_n + \Delta t_n$ by the following algorithm:

1. Solve the Navier-Stokes equations (35) for \mathbf{u}_L and p .
2. Recover the pressure gradient ∇p using an L_2 -projection.
3. Calculate the slip velocity as $\mathbf{u}_{\text{slip}} = -\frac{\nabla p}{C_W}$.
4. Advance $\tilde{\rho}_G$ using (41) and recompute $\epsilon = \frac{\tilde{\rho}_G RT}{p\eta}$.
5. Substitute ϵ into (35) and evaluate the residual.
6. If converged then proceed to 7, otherwise go to 1.
7. Update the number density n according to (37).
8. Solve the homogeneous transport equations (42)–(44).
9. Compute the interfacial area $a_S = (4\pi n)^{1/3} (3\epsilon)^{2/3}$.
10. Solve the ODE system (45)–(48) for each node.

An implicit time discretization of Crank-Nicolson or backward Euler type is employed for all equations. The value of the implicitness parameter θ and of the local time step can be selected individually for each subproblem so as to maximize accuracy and/or stability. This provides an efficient treatment of physical processes occurring simultaneously but on entirely different time scales. The communication between the subproblem blocks takes place at the end of the common macro time step Δt_n which is chosen adaptively so as to control the changes of the gas holdup distribution (see below). The linear systems are solved using preconditioned BiCGSTAB or multigrid methods. In what follows, we elucidate some constituents of the numerical algorithm in detail.

3.1 Treatment of incompressibility

The Boussinesq system (35) is solved using the academic code FEATFLOW [27]. This open-source software package represents a collection of robust discretization tools and optimized multigrid solvers for incompressible flow problems. Below, we briefly outline the Pressure Schur Complement method adopted for gas-liquid flow simulations.

The fully discretized Navier-Stokes equations represent a saddle point problem, in which the pressure acts as a Lagrange multiplier for the incompressibility constraint:

$$\begin{bmatrix} S & \Delta t B \\ B^T & 0 \end{bmatrix} \begin{bmatrix} \mathbf{u} \\ p \end{bmatrix} = \begin{bmatrix} \mathbf{f} \\ 0 \end{bmatrix}. \quad (49)$$

The velocity can be formally written as $\mathbf{u} = S^{-1}(\mathbf{f} - \Delta t B p)$ and plugged into the discrete continuity equation $B^T \mathbf{u} = 0$ to derive the missing equation for the pressure:

$$B^T S^{-1} B p = \Delta t^{-1} B^T S^{-1} \mathbf{f}. \quad (50)$$

This discrete problem can be solved by the preconditioned Richardson iteration [26]

$$p^{(l+1)} = p^{(l)} + [B^T M_L^{-1} B]^{-1} \Delta t^{-1} B^T S^{-1} (\mathbf{f} - \Delta t B p^{(l)}), \quad (51)$$

where l is the outer iteration counter and M_L is the lumped mass matrix which proves to be a reasonable approximation to the evolution operator S at high Reynolds numbers.

Each Pressure Schur Complement iteration can be interpreted and implemented as a projection cycle which consists of the following algorithmic steps:

1. Compute the velocity $\tilde{\mathbf{u}}$ from the Burgers equation

$$S \tilde{\mathbf{u}} = \mathbf{f} - \Delta t B p^{(l)}$$

2. Solve the discrete ‘Pressure-Poisson’ problem

$$B^T M_L^{-1} B q = \Delta t^{-1} B^T \tilde{\mathbf{u}}$$

3. Correct the pressure and the intermediate velocity

$$p^{(l+1)} = p^{(l)} + q, \quad \mathbf{u}^{(l+1)} = \tilde{\mathbf{u}} - \Delta t M_L^{-1} B q$$

In a nutshell, the right-hand side of the momentum equation is assembled using the old pressure iterate and the resulting intermediate velocity $\tilde{\mathbf{u}}$ is projected onto the subspace of divergence-free functions so as to satisfy the condition $B^T \mathbf{u}^{(l+1)} = 0$. The Pressure Schur Complement approach constitutes a very general framework which unites coupled solution techniques and classical projection schemes, the degree of coupling being determined by the number of outer iterations. For details the interested reader is referred to [29].

3.2 Treatment of convection

Convection is notoriously difficult to treat numerically. The standard Galerkin method is a ‘centered’ scheme which gives rise to an unstable discretization of convective terms. A common remedy is to add streamline diffusion which provides the necessary stabilization without reducing the order of approximation. However, even stabilized high-order methods tend to produce nonphysical undershoots and overshoots in the vicinity of steep gradients. As a result, negative gas holdups or concentrations may arise, which is clearly unacceptable. It is possible to get rid of oscillations by adding adaptive artificial diffusion depending on the local solution behavior. The high-order scheme can be used in smooth regions but near discontinuities it should be replaced by a low-order scheme like ‘upwind’ which is diffusive enough to prevent the formation of wiggles.

The first discretization procedure to utilize the idea of adaptive switching between high- and low-order methods was the flux-corrected-transport algorithm introduced in the early 1970s by Boris and Book [3]. The state-of-the-art generalization proposed by Zalesak [33] has made it possible to incorporate FCT into unstructured grid methods. The foundations of flux correction for finite elements were laid by Löhner *et al.* [17]. In a series of recent publications [11], [13], [14] we refined the FEM-FCT methodology and extended it to implicit time stepping. Unfortunately, Zalesak’s limiter leads to some loss of accuracy for large time steps, which compromises the advantages of implicit schemes.

A class of high-resolution methods with artificial diffusion independent of the time step was developed by Harten [7]. His total variation diminishing schemes and extensions thereof rest on a firm mathematical basis and are widely used in CFD computations. At the same time, it has been largely unclear how to apply them in the finite element context. In the scarce publications on that subject, TVD-like artificial viscosities were designed using some reconstruction of a local 1D stencil [18]. The use of P_1 elements was essential to the derivation of the underlying edge-based data structure. Below we propose an alternative approach which is applicable to arbitrary Galerkin discretizations. The (anti-)diffusive terms are represented as an array of internodal fluxes. A complete transition to an edge-based data structure is feasible [14] but not mandatory.

3.2.1 Galerkin discretization

Consider a time-dependent conservation law for a scalar quantity u :

$$\frac{\partial u}{\partial t} + \nabla \cdot (\mathbf{f} - d\nabla u) = 0 \quad \text{in } \Omega, \quad (52)$$

where $\mathbf{f} = \mathbf{v}u$ stands for the convective flux and d denotes the diffusion coefficient. All of our homogeneous transport equations (37), (41)–(44) can be written in this form.

The concomitant boundary conditions are specified in terms of normal fluxes:

$$\begin{aligned} -\mathbf{n} \cdot (\mathbf{f} - d\nabla u) &= g \quad \text{on } \Gamma_1, \\ \mathbf{n} \cdot (\mathbf{f} - d\nabla u) &= 0 \quad \text{on } \Gamma_2, \\ \mathbf{n} \cdot \nabla u &= 0 \quad \text{on } \Gamma_3, \end{aligned}$$

where \mathbf{n} denotes the outward unit normal. On the feed boundary Γ_1 the incoming flux is determined by the operating conditions. In particular, the total gas throughput divided by the aerated area yields the value of g for the continuity equation (41). Obviously, there is no flux through the solid wall Γ_2 . On the outflow boundary Γ_3 the diffusive flux is cancelled while the convective one is left free as required by the hyperbolic limit of pure convection ($d = 0$). It is implied that $\mathbf{v} \cdot \mathbf{n} < 0$ on Γ_1 while $\mathbf{v} \cdot \mathbf{n} > 0$ on Γ_3 .

Using the divergence theorem to integrate the spatial derivatives in the weak form of equation (52) by parts and inserting the natural boundary conditions, we obtain

$$\int_{\Omega} w \frac{\partial u}{\partial t} d\mathbf{x} - \int_{\Omega} \nabla w \cdot (\mathbf{f} - d\nabla u) d\mathbf{x} + \int_{\Gamma_3} w \mathbf{f} \cdot \mathbf{n} ds = \int_{\Gamma_1} wg ds. \quad (53)$$

A common practice in finite element methods for conservation laws is to interpolate the fluxes in the same way as the approximate solution:

$$u_h = \sum_j u_j \varphi_j, \quad \mathbf{f}_h = \sum_j \mathbf{f}_j \varphi_j = \sum_j (\mathbf{v}_j u_j) \varphi_j, \quad (54)$$

where φ_i are the basis functions spanning the finite-dimensional subspace. The resulting Galerkin discretization of equation (52) reads

$$\begin{aligned} \sum_j \left[\int_{\Omega} \varphi_i \varphi_j d\mathbf{x} \right] \frac{du_j}{dt} - \sum_j \left[\int_{\Omega} \nabla \varphi_i \cdot (\mathbf{v}_j \varphi_j - d\nabla \varphi_j) d\mathbf{x} \right] u_j \\ + \sum_j \left[\int_{\Gamma_3} \varphi_i \varphi_j \mathbf{v}_j \cdot \mathbf{n} ds \right] u_j = \int_{\Gamma_1} \varphi_i g ds. \end{aligned} \quad (55)$$

This ODE system can be written in compact matrix form as follows

$$M_C \frac{du}{dt} = (K - B)u + q, \quad (56)$$

where M_C is the consistent mass matrix, K is the discrete transport operator, B is the contribution of the surface integral over the Neumann boundary and q is the source term due to incoming fluxes. The matrix entries are given by

$$m_{ij} = \int_{\Omega} \varphi_i \varphi_j d\mathbf{x}, \quad k_{ij} = \mathbf{v}_j \cdot \mathbf{c}_{ij} - d s_{ij}, \quad (57)$$

where \mathbf{c}_{ij} and s_{ij} stand for the constant coefficients

$$\mathbf{c}_{ij} = \int_{\Omega} \nabla \varphi_i \varphi_j d\mathbf{x}, \quad s_{ij} = \int_{\Omega} \nabla \varphi_i \cdot \nabla \varphi_j d\mathbf{x}. \quad (58)$$

corresponding to the first- and second-order derivatives, respectively. For customary finite elements, the sum of basis functions is identically one so that the sum of their derivatives vanishes. Hence, the above coefficient matrices have zero column sums and so does the discrete transport operator: $\sum_i k_{ij} = \mathbf{v}_j \cdot \sum_i \mathbf{c}_{ij} - d \sum_i s_{ij} = 0$.

Note that the differential operators defined by equation (58) do not change and need to be assembled just once. As long as they are available, the matrix K can be updated in an efficient way by computing the off-diagonal entries k_{ij} from the formula (57) without resorting to costly numerical integration. Due to the zero column sum property, the diagonal matrix entries can be recovered as $k_{jj} = -\sum_{i \neq j} k_{ij}$.

The boundary terms are assembled separately. It is expedient to calculate the surface integrals approximately using a one-point quadrature rule. For each boundary edge/face ∂E_k we evaluate the normal flux at the midpoint, multiply it by the respective area $|\partial E_k|$ and distribute between the nodes. This leads to a diagonal matrix B with entries

$$b_i = \frac{1}{m} \sum_{k \in \mathcal{J}_1^i} \mathbf{v}_i \cdot \mathbf{n}_k |\partial E_k|, \quad \mathcal{J}_1^i = \{j : \mathbf{x}_i \in \partial E_j \cap \Gamma_1\}, \quad (59)$$

where m denotes the number of local degrees of freedom per edge/face and \mathbf{n}_k is the (unique) outward normal to ∂E_k . The source term is assembled in a similar way:

$$q_i = \frac{1}{m} \sum_{k \in \mathcal{J}_3^i} g_k |\partial E_k|, \quad \mathcal{J}_3^i = \{j : \mathbf{x}_i \in \partial E_j \cap \Gamma_3\}. \quad (60)$$

Clearly, q does not have to be recomputed as long as the boundary conditions are fixed.

An important advantage of using piecewise-constant normal fluxes in the assembly process is that the disjoint boundary components $\Gamma_1, \Gamma_2, \Gamma_3$ are unambiguously defined and the boundary conditions are allowed to have a jump at the interface.

3.2.2 Construction of a linear LED scheme

Let us perform mass lumping and represent the semi-discrete problem in the form

$$M_L \frac{du}{dt} = (K - B)u + q \quad \Leftrightarrow \quad m_i \frac{du_i}{dt} = \sum_{j \neq i} k_{ij} (u_j - u_i) + r_i u_i + q_i, \quad (61)$$

where $m_i = \sum_j m_{ij}$ and $r_i = \sum_j k_{ij} - b_i$. The term $r_i u_i$ is a discrete counterpart of $u \nabla \cdot \mathbf{v}$ which vanishes for incompressible flows. It is instructive to consider the special case $r_i = q_i = 0$ in which the discrete transport operator K has zero row sum. Such a discretization would be local extremum diminishing [8] if all off-diagonal coefficients k_{ij} were nonnegative. Indeed, if u_i is a maximum, then $k_{ij}(u_j - u_i) \leq 0$, so that $\frac{du_i}{dt} \leq 0$. Hence, a maximum cannot increase, and similarly a minimum cannot decrease. In one dimension, a LED scheme is total variation diminishing and monotonicity preserving.

The Galerkin transport operator K can be rendered LED by adding a tensor of artificial diffusion D designed so as to eliminate negative off-diagonal entries [13], [14]

$$L = K + D, \quad d_{ii} = -\sum_{k \neq i} d_{ik}, \quad d_{ij} = d_{ji} = \max\{0, -k_{ij}, -k_{ji}\}. \quad (62)$$

The diffusion coefficients d_{ij} are associated with the edges of the graph representing the connectivity of the matrix. For each pair of neighboring nodes i and j , a negative off-diagonal coefficient (say, k_{ij}) is set to zero, while its mirror image k_{ji} is incremented by

$-k_{ij}$ and the diagonal entries k_{ii}, k_{jj} are updated so as to maintain zero column sums. This yields the least diffusive linear LED scheme which reduces to the standard upwind approximation for scalar convection problems in one dimension [13]. The row number of the nullified off-diagonal entry determines which of the two nodes is located ‘upwind’. Without loss of generality, we will assume that i is the upwind node for the numerical edge \vec{ij} , so that $l_{ij} = 0$ whereas $l_{ji} = |k_{ji} - k_{ij}|$. The diffusive flux $d_{ij}(u_j - u_i)$ reduces the difference between the nodal values so as to enforce the positivity constraint.

Note that the artificial diffusion coefficients d_{ij} as defined in (62) are independent of the diagonal part r_i which allows for the physical growth and decay of extrema due to compressibility. The boundary terms q_i are assumed to be nonnegative and may only increase the value of u in the interior. Physical diffusion (if any) built into the coefficients k_{ij} is automatically detected and the amount of artificial diffusion is reduced accordingly. Alternatively, discrete upwinding can be performed only for the convective part of K .

3.2.3 Defect correction

According to the well-known Godunov theorem, linear monotonicity preserving schemes can be at most first order accurate. To obtain a nonlinear high-resolution scheme, we combine the Galerkin discretization and the associated low-order method within an iterative defect correction loop for the fully discretized problem:

$$u^{(l+1)} = u^{(l)} + \omega^{(l)}[C(u^{(l)})]^{-1}R(u^{(l)}), \quad l = 0, 1, 2, \dots \quad (63)$$

In a practical implementation one solves a linear subproblem for the solution increment and applies the weighted correction to the last iterate:

$$C(u^{(l)})\Delta u^{(l)} = R(u^{(l)}), \quad u^{(l+1)} = u^{(l)} + \omega^{(l)}\Delta u^{(l)}, \quad u^{(0)} = u^n. \quad (64)$$

Specifically, we take the ‘preconditioner’ to be the low-order evolution operator

$$C(u^{(l)}) = M_L - \theta\Delta t L(u^{(l)}), \quad 0 \leq \theta \leq 1,$$

where θ is the implicitness parameter. By construction, C is an M-matrix which makes it amenable to iterative solution. The residual vector is given by

$$R(u^{(l)}) = M_L(u^n - u^{(l)}) + \theta\Delta t[L(u^{(l)}) - A(u^{(l)})]u^{(l)} + (1 - \theta)\Delta t[L(u^n) - A(u^n)]u^n + q^{n+\theta},$$

where A is a nonlinear antidiffusion operator to be defined below.

The difference between $K^* = L - A = K + D - A$ and the original transport operator K is a matrix with zero row and column sums. Hence, the diffusive-antidiffusive terms can be decomposed into skew-symmetric internodal fluxes:

$$(K^*u)_i = \sum_j k_{ij}u_j + \sum_{j \neq i} (f_{ij}^d + f_{ij}^a), \quad \text{where} \quad f_{ij}^d = d_{ij}(u_j - u_i) = -f_{ji}^d. \quad (65)$$

The antidiffusive flux f_{ij}^a from node j into node i is designed so as to comply with the LED principle for the discrete scheme. The objective is to add as much antidiffusion as possible without generating wiggles. This can be accomplished by applying flux limiters of TVD and FCT type presented in the next two subsections.

3.2.4 TVD flux limiter

For the discrete scheme to be LED, the antidiffusive flux f_{ij}^a must be interpretable as a diffusive flux from some other node(s). To provide this property, we may consider

$$f_{ij}^a = a_{ij}\mathcal{L}(1, \theta_i)(u_i - u_j) = a_{ij}\mathcal{L}(u_i - u_j, \Delta u_{ij}), \quad f_{ji}^a = -f_{ij}^a. \quad (66)$$

Extra antidiffusion due to the consistent mass matrix can be included and limited as in the FEM-FCT framework (see below). Let us leave the antidiffusion coefficient a_{ij} and the difference $\Delta u_{ij} = \theta_i(u_i - u_j)$ unspecified for the time being. The flux limiter \mathcal{L} represents a limited average operator satisfying certain properties which guarantee the positivity of coefficients [8], [18]. In particular, $\mathcal{L}(a, b) = 0$ if a and b have opposite sign. Another useful property is symmetry: $\mathcal{L}(a, b) = \mathcal{L}(b, a)$. Some popular TVD limiters are:

- $\mathcal{L}(a, b) = \mathcal{S}(a, b) \cdot \min\{|a|, |b|\}$ minmod
- $\mathcal{L}(a, b) = \mathcal{S}(a, b) \cdot \frac{2ab}{|a+b|}$ Van Leer
- $\mathcal{L}(a, b) = \mathcal{S}(a, b) \cdot \min\left\{\frac{|a+b|}{2}, 2|a|, 2|b|\right\}$ 2-mean
- $\mathcal{L}(a, b) = \mathcal{S}(a, b) \cdot \max\{\min\{2|a|, |b|\}, \min\{|a|, 2|b|\}\}$ superbee

where $\mathcal{S}(a, b) = (\text{sign}(a) + \text{sign}(b))/2$.

Recall that the numerical edge $\vec{i}j$ connects an upwind node i and a downwind node j . Its contributions to the modified convective term can be written as

$$\begin{aligned} \text{node } i : \quad & k_{ij}^*(u_j - u_i) = a_{ij}\mathcal{L}(1, \theta_i)(u_i - u_j) = a_{ij}\mathcal{L}(1, 1/\theta_i)\Delta u_{ij}, \\ \text{node } j : \quad & k_{ji}^*(u_i - u_j) = (|k_{ji} - k_{ij}| - a_{ij}\mathcal{L}(1, \theta_i))(u_i - u_j). \end{aligned}$$

The increment to node j exhibits a LED structure provided that the coefficient k_{ji}^* is nonnegative. All of the flux limiters presented above satisfy the inequality $0 \leq \mathcal{L}(1, \theta) \leq 2$. Hence, the antidiffusion coefficient is taken to be

$$a_{ij} = \min\{d_{ij}, |k_{ji} - k_{ij}|/2\}. \quad (67)$$

The increment to node i will also be local extremum diminishing as long as the upwind difference Δu_{ij} can be cast in the form $\Delta u_{ij} = \sum_{k \neq i} c_{ik}(u_k - u_i)$ with $c_{ik} \geq 0$.

In one-dimensional TVD schemes, θ_i represents the slope ratio at the upwind node, so that $\Delta u_{ij} = u_k - u_i$, where $k \neq j$ refers to the second neighbor of node i . However, the choice of Δu_{ij} for finite element discretizations on unstructured meshes is nontrivial. A geometric approach commonly employed in the literature is to reconstruct a local one-dimensional stencil by introducing two dummy nodes on the continuation of the edge $\vec{i}j$ [8], [18]. The difference Δu_{ij} is defined as in the 1D case using the interpolated or extrapolated solution value at the dummy node k adjacent to the upwind node.

A detailed comparison of various techniques for the recovery of u_k can be found in [18]. It was shown that the numerical results strongly depend on the employed procedure. In particular, those obtained by means of the gradient reconstruction

$$\Delta u_{ij} = (\mathbf{x}_i - \mathbf{x}_j) \cdot \nabla_h u_i, \quad \text{where} \quad \nabla_h u_i = \frac{1}{m_i} \sum_{k \neq i} \mathbf{c}_{ki} (u_k - u_i) \quad (68)$$

were found to be quite poor. It is quite clear why this choice of the upwind difference may fail to produce non-oscillatory results. The L_2 -projection of the discrete gradient using Galerkin differential operators is not monotone. Some of the coefficients in the formula for Δu_{ij} may be negative, so that it will not possess the desired form. To rectify this, we employ a low-order projection operator designed by resorting to discrete upwinding as proposed above. Note that $\mathbf{c}_{ki} = -\mathbf{c}_{ik}$ (for internal nodes), so that the elimination of negative off-diagonal coefficients leads to the following LED-type expression:

$$\Delta u_{ij} = \frac{2}{m_i} \sum_{k \neq i} \max\{0, \mathbf{c}_{ki} \cdot (\mathbf{x}_i - \mathbf{x}_j)\} (u_k - u_i).$$

For uniform meshes in one dimension, this kind of extrapolation corresponds to using the upwind gradient and yields the standard value $\Delta u_{ij} = u_k - u_i$.

3.2.5 FCT flux limiter

As an alternative, we outline another flux limiter based on the generalized FEM-FCT formulation [11], [13]. In this case, the raw antidiffusion is given by

$$f_{ij} = a_{ij}^{(l)} (u_i^{(l)} - u_j^{(l)}) + a_{ij}^n (u_i^n - u_j^n), \quad f_{ji} = -f_{ij}, \quad (69)$$

where

$$a_{ij}^{(l)} = m_{ij} + \theta \Delta t d_{ij}^{(l)}, \quad a_{ij}^n = -m_{ij} + (1 - \theta) \Delta t d_{ij}^n. \quad (70)$$

Solution-dependent correction factors $\alpha_{ij} \in [0, 1]$ are applied to f_{ij} in order to preclude the arising of nonphysical oscillations. The admissible antidiffusive fluxes $f_{ij}^a = \alpha_{ij} f_{ij}$ are inserted into the defect vector $R(u^{(l)})$ to reduce the errors induced by mass lumping and discrete upwinding. The unified limiting strategy proposed in [11], [13] is as follows.

At the beginning of each time step, the explicit subproblem

$$M_L \tilde{u} = [M_L + (1 - \theta) \Delta t L(u^n)] u^n \quad (71)$$

is solved for \tilde{u} to determine the local extrema \tilde{u}_i^{\max} and \tilde{u}_i^{\min} . Note that the auxiliary solution \tilde{u} is associated with the time instant $t^{n+1-\theta}$ and reduces to u^n for the backward Euler method. Following Zalesak [33], we introduce

$$P_i^\pm = \frac{1}{m_i} \sum_{j \neq i} \max\{0, f_{ij}\}, \quad Q_i^\pm = \tilde{u}_i^{\max} - \tilde{u}_i. \quad (72)$$

For the scheme to be positivity-preserving, the flux into node i should be multiplied by

$$R_i^\pm = \begin{cases} \min\{1, Q_i^\pm / P_i^\pm\}, & \text{if } P_i^\pm \neq 0, \\ 0, & \text{if } P_i^\pm = 0. \end{cases} \quad (73)$$

Due to the fact that $f_{ji} = -f_{ij}$ the ‘optimal’ correction factors are given by

$$\alpha_{ij} = \begin{cases} \min\{R_i^+, R_j^-\}, & \text{if } f_{ij} \geq 0, \\ \min\{R_j^+, R_i^-\}, & \text{if } f_{ij} < 0. \end{cases} \quad (74)$$

The ins and outs of the FEM-FCT methodology are elucidated in [13], [14], [16].

3.3 Solver and time step

Finally, let us briefly discuss the choice of the iterative solver and of the time discretization. In general, explicit schemes are rather inefficient due to severe stability limitations which require taking impractically small time steps. For this reason, we restrict ourselves to the implicit Crank-Nicolson and backward Euler methods which are unconditionally stable and permit large time steps at the expense of solving nonsymmetric linear systems.

In our experience, BiCGSTAB and geometric multigrid constitute excellent solvers as long as the parameters are properly tuned and the underlying smoothers/preconditioners are consistent with the size of the time step. If Δt is rather small, standard components like Jacobi, Gauß-Seidel and SOR schemes will suffice. For large time steps, the condition number of the matrix deteriorates and convergence may fail. This can be rectified by resorting to an ILU factorization in conjunction with an appropriate renumbering scheme.

In order to capture the dynamics of the two-phase flow in a computationally efficient way, one needs a smart strategy for the time step control. So far we have used a fairly simple PID controller due to Valli *et al.* [30]. In our case, the algorithm reads

1. Monitor the relative changes of the gas holdup distribution

$$e_n = \frac{\|\epsilon^{n+1} - \epsilon^n\|}{\|\epsilon^{n+1}\|}$$

2. If $e_n > \delta$ reject the solution and repeat the time step using

$$\Delta t_* = \frac{\delta}{e_n} \Delta t_n$$

3. Adjust the time step smoothly so as to approach the prescribed tolerance for the relative changes

$$\Delta t_{n+1} = \left(\frac{e_{n-1}}{e_n}\right)^{k_P} \left(\frac{TOL}{e_n}\right)^{k_I} \left(\frac{e_{n-1}^2}{e_n e_{n-2}}\right)^{k_D} \Delta t_n$$

4. Limit the growth and reduction of the time step so that

$$\Delta t_{\min} \leq \Delta t_{n+1} \leq \Delta t_{\max}, \quad m \leq \frac{\Delta t_{n+1}}{\Delta t_n} \leq M$$

Note that the local gas holdup ϵ is a perfect indicator variable because the bubble-induced buoyancy represents a major driving force behind the flows in gas-liquid reactors.

4 Numerical examples

The developed finite element software builds on the FEATFLOW package [27] and on the underlying FEAT libraries [28]. The multidimensional TVD limiter was incorporated into the matrix assembly routine for the momentum equation and has proved its worth for the nonconforming \tilde{Q}_1 finite elements. The subroutines for the solution of scalar transport equations were equipped with both FCT and TVD limiters. The performance of these high-resolution schemes was found to be similar. Let us substantiate the mathematical model and the numerical algorithm by preliminary simulation results.

The first example deals with the startup of a locally aerated cylindrical bubble column. The gas is injected at the center into the initially quiescent liquid. The buoyancy induced by the ascending bubbles results in a circulation of liquid with upflow in the middle. The evolution of the gas holdup distribution during the first seconds after the onset of aeration is shown in Figure 1 along with fragments of the employed computational mesh. Similar mushroom-like shapes were observed previously in 2D simulations [10], [15], [25].

Next, we present our three-dimensional results for the airlift loop reactor which was investigated both experimentally and numerically by Becker *et al.* [1]. The aeration takes place at the bottom of the riser section where both phases flow cocurrently in the upward direction. At the upper surface, the bubbles escape while the liquid is diverted into the

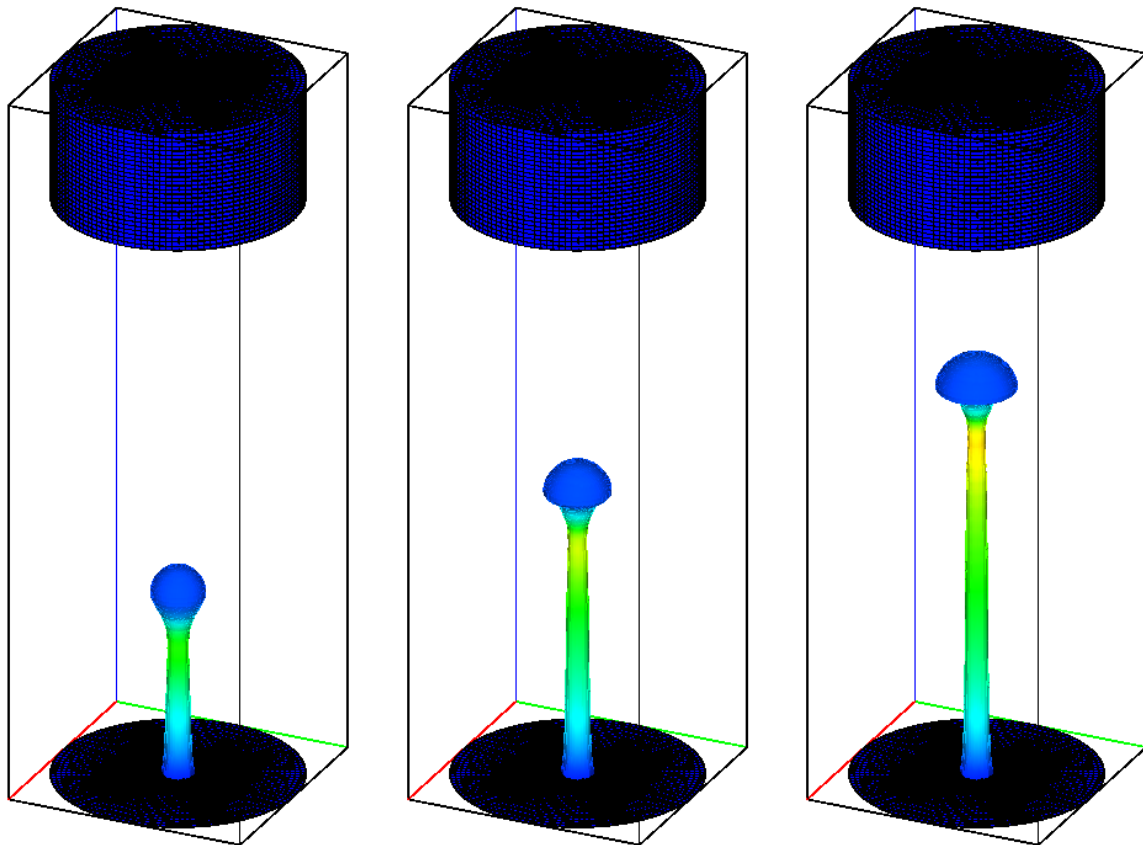


Figure 1. Startup of a locally aerated cylindrical bubble column.

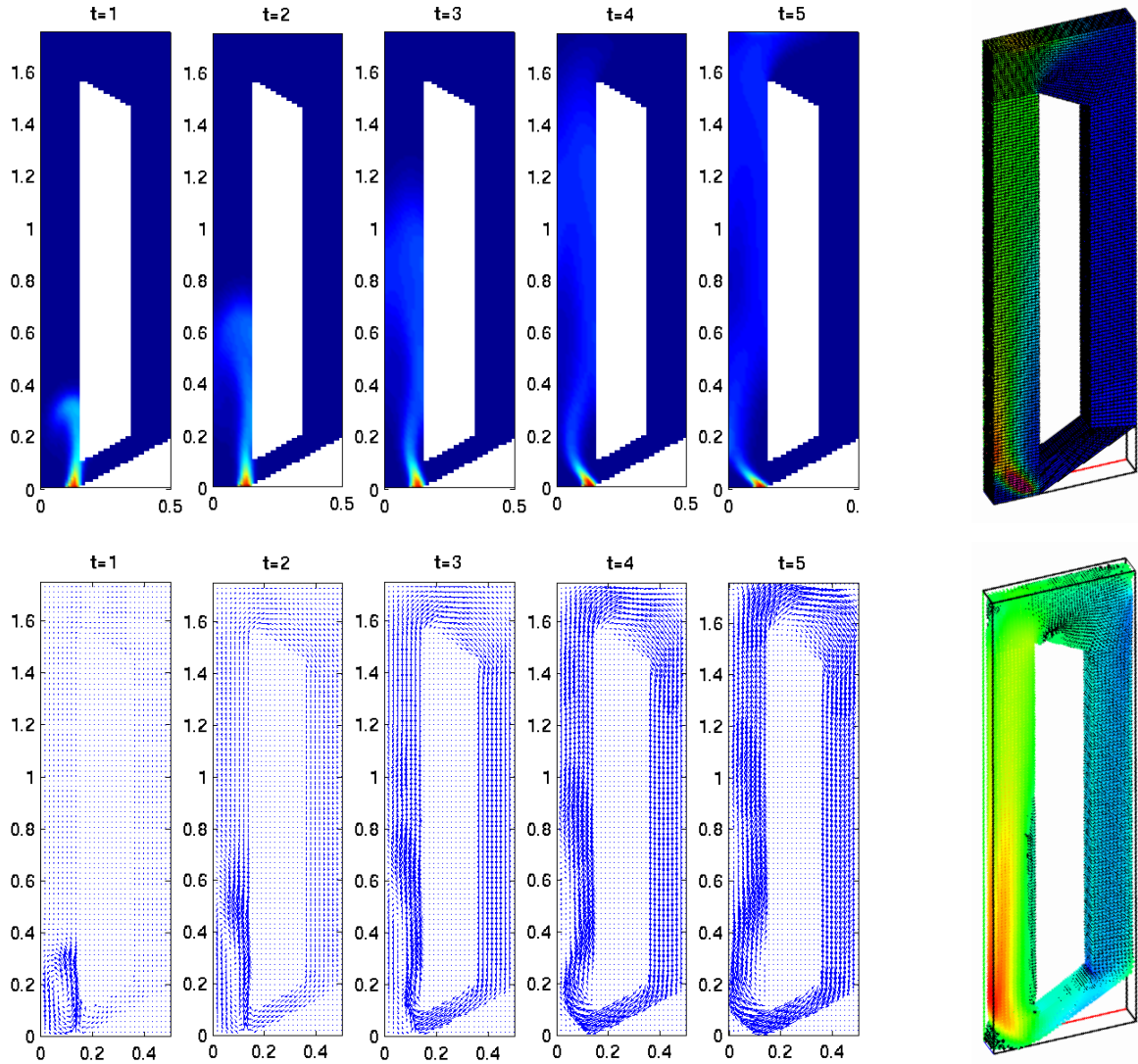


Figure 2. Airlift loop reactor: startup (left) and steady state (right).

gas-free downcomer forming a closed loop. The two-phase flow reaches a steady state within a few seconds after the startup of the reactor. Figure 2 (left) displays snapshots of the developing gas holdup distribution (top) and instantaneous velocity fields (bottom) in the middle cross section. The ragged boundary of the internal part is due to the Cartesian mesh used for visualization. The three-dimensional stationary solution superimposed on the actual block-structured computational mesh is shown on the right.

To give an insight into the complex interplay of physical and chemical phenomena, let us consider the absorption of CO_2 in a locally aerated bubble column filled with water. The construction parameters are those defined by Becker *et al.* [1] and adopted in our first 2D simulations for this test case [10], [12]. In the absence of mass transfer, the rising bubbles would expand due to the fall of hydrostatic pressure. However, carbon dioxide is highly soluble in water so that the growth is diminished and the bubbles may even shrink.

These effects are nicely reproduced by our model. In the case of physical absorption, the gas dissolves rather slowly and neither the instantaneous gas holdup distribution (Figure 3, top) nor the velocity fields (Figure 3, middle) are significantly affected by the absorption process [10]. The flow structure consisting of three large vortices is reflected by the concentration fields for the dissolved carbon dioxide (Figure 3, bottom).

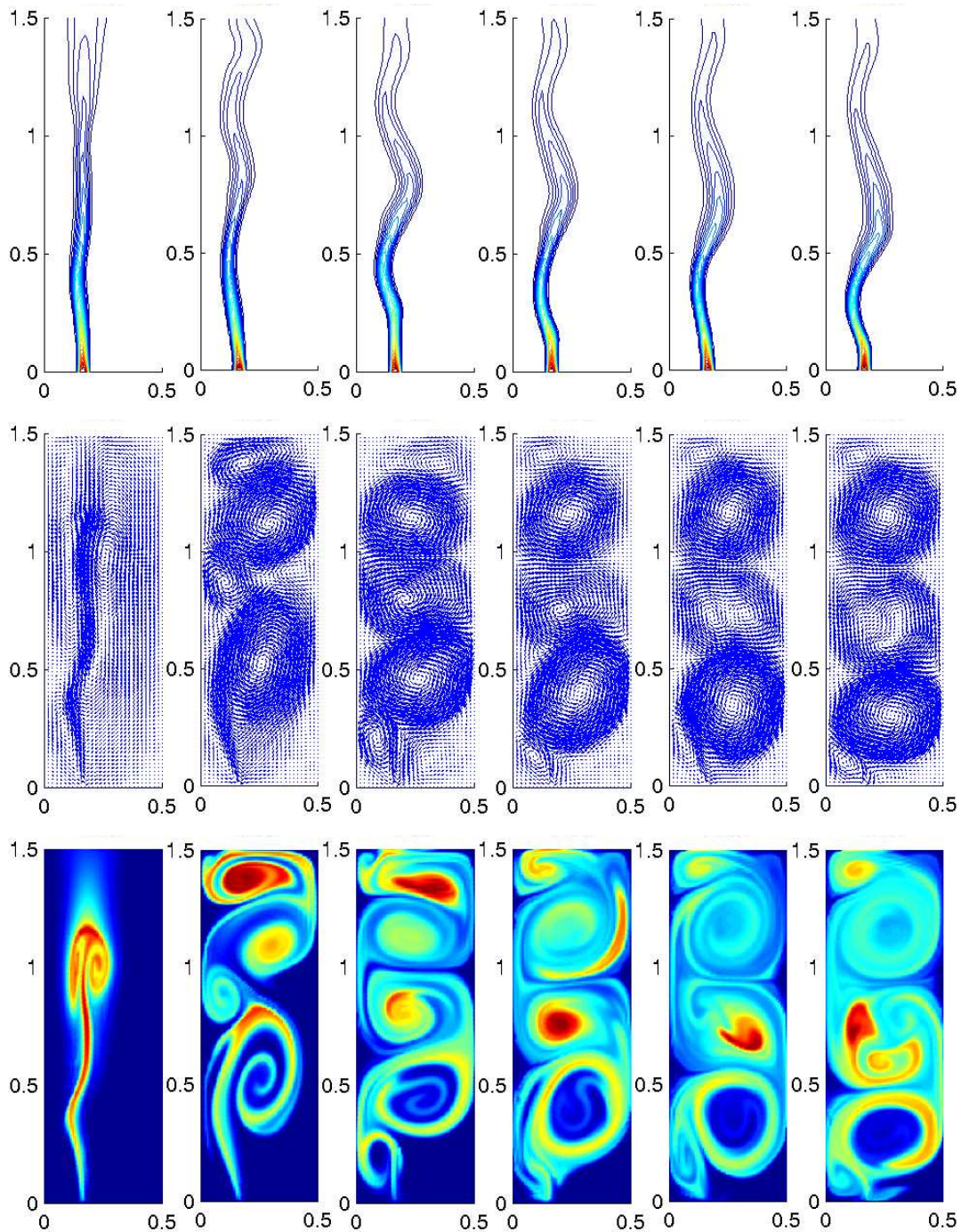


Figure 3. Physical absorption of CO₂ (2D simulation).

The flow pattern is totally different if the mass transfer is accelerated by chemical reactions in the liquid phase. Let us demonstrate this by taking an aqueous solution of sodium hydroxide instead of water. The reaction $\text{CO}_2 + 2\text{NaOH} \rightarrow \text{Na}_2\text{CO}_3 + \text{H}_2\text{O}$ is so fast that the bubbles are completely dissolved within 20 cm from the inlet (Figure 4, top). There is no liquid circulation in the upper part of the reactor since the gas does not reach

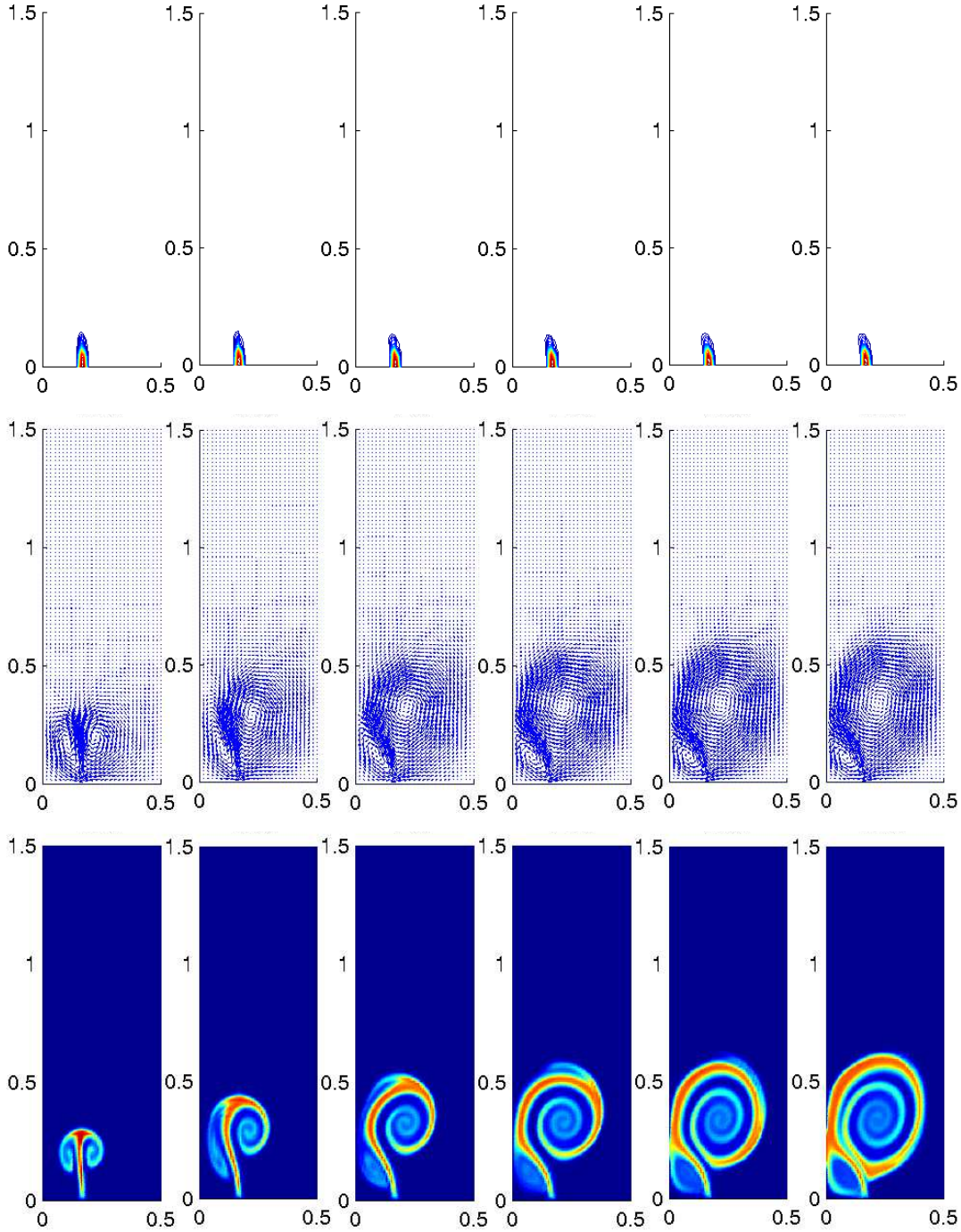


Figure 4. Reaction-enhanced absorption of CO₂ (2D simulation).

it. A large vortex develops in the vicinity of the gas sparger (Figure 4, middle) twisting the concentration of the produced sodium carbonate into a spiral shape (Figure 4, bottom). A 3D simulation predicts essentially the same flow behavior depicted in Figure 5. The results are in good agreement with experimental data reported by Fleischer *et al.* [6].

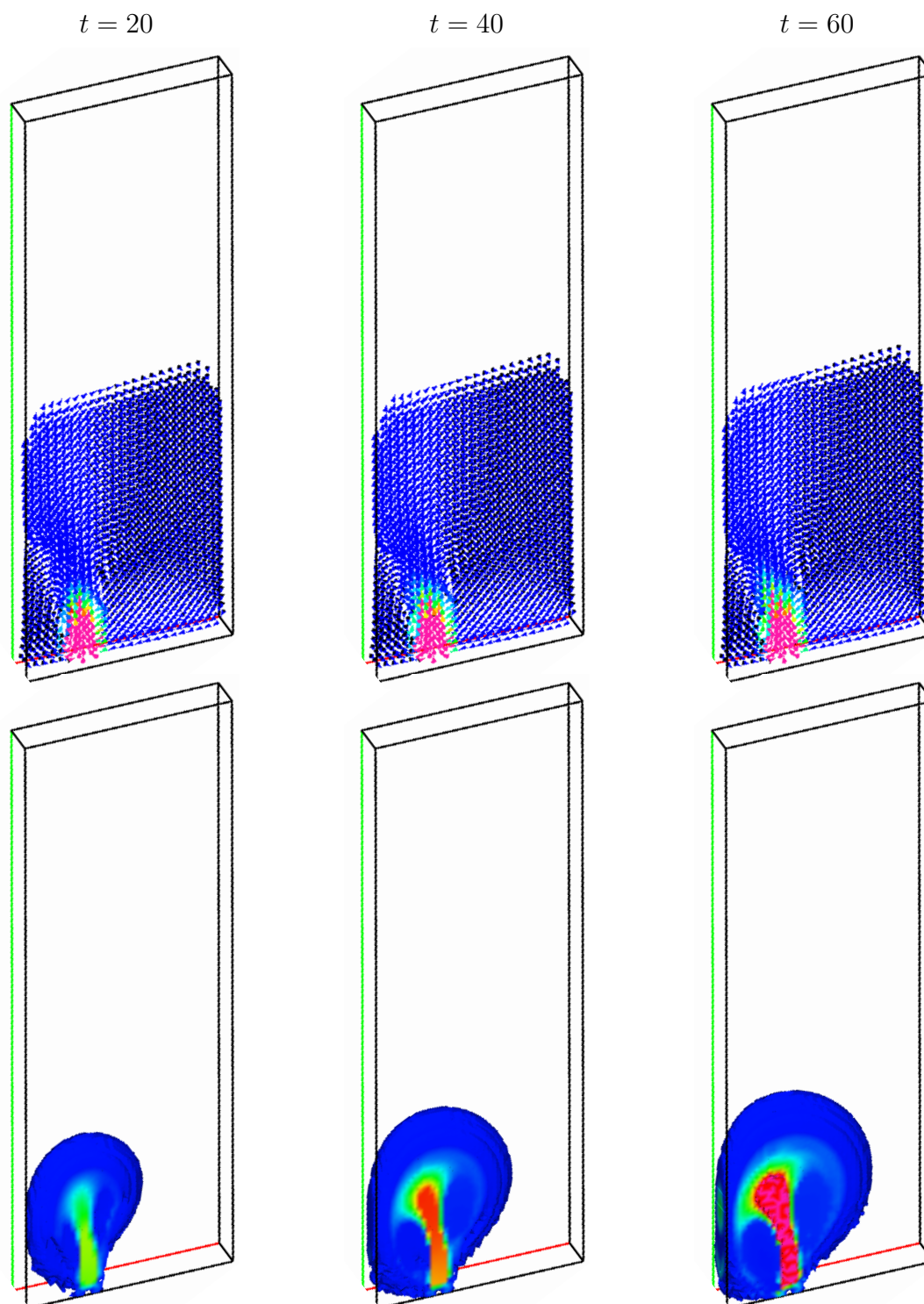


Figure 5. Reaction-enhanced absorption of CO_2 (3D simulation).

5 Conclusions

The drift-flux model for buoyancy-driven bubbly flows was coupled with scalar transport equations describing the absorption of gas followed (and enhanced) by chemical reactions in the liquid phase. An unstructured grid finite element method was proposed for the numerical solution. The discretization of the troublesome convective terms was performed by a novel high-resolution scheme. Nested iterations were used to provide the coupling of model equations, get rid of nonlinearities and solve the linear systems. The subtleties of the algorithm were discussed in detail. The strong interdependence of the hydrodynamics, mass transfer and chemical reaction processes was illustrated by numerical examples. Turbulence effects were not considered and will be addressed in a forthcoming paper.

References

- [1] S. Becker, A. Sokolichin and G. Eigenberger, Gas-liquid flow in bubble columns and loop reactors: Part II. Comparison of detailed experiments and flow simulations. *Chem. Eng. Sci.* **49** (1994), no. 24B, 5747–5762.
- [2] O. Borchers, C. Busch, A. Sokolichin, and G. Eigenberger, Applicability of the standard turbulence model to the dynamic simulation of bubble columns: Part II. Comparison of detailed experiments and flow simulations. *Chem. Eng. Sci.* **54** (1999) 5927-5935.
- [3] J. P. Boris and D. L. Book, Flux-corrected transport. I. SHASTA, A fluid transport algorithm that works. *J. Comput. Phys.* **11** (1973) 38–69.
- [4] D. A. Drew, Mathematical modeling of two-phase flow. *Ann. Rev. Fluid Mech.* **15** (1983) 261-291.
- [5] D. A. Drew and S. L. Passman, *Theory of Multicomponent Fluids*. Springer, 1999.
- [6] C. Fleischer, S. Becker and G. Eigenberger, Detailed modeling of the chemisorption of CO₂ into NaOH in a bubble column. *Chem. Eng. Sci.* **51** (1996), no. 10, 1715–1724.
- [7] A. Harten, High resolution schemes for hyperbolic conservation laws, *J. Comput. Phys.* **49** (1983) 357–393.
- [8] A. Jameson, Positive schemes and shock modelling for compressible flows. *Int. J. Numer. Methods Fluids* **20** (1995) 743–776.
- [9] I. Kataoka and A. Serizawa, Basic equations of turbulence in gas-liquid two-phase flow. *Int. J. Multiphase Flow* **15** (1989) 843-855.
- [10] D. Kuzmin, *Numerical Simulation of Reactive Bubbly Flows*. Dissertation, Jyväskylä Studies in Computing 2, University of Jyväskylä, 1999.
- [11] D. Kuzmin, Positive finite element schemes based on the flux-corrected transport procedure, In: *Computational Fluid and Solid Mechanics*, Elsevier, 887-888 (2001).

- [12] D. Kuzmin and S. Turek, Efficient numerical techniques for flow simulation in bubble column reactors. In: *Preprints of the 5th German-Japanese Symposium on Bubble Columns*, VDI/GVC, 2000, 99-104.
- [13] D. Kuzmin and S. Turek, Flux correction tools for finite elements. *J. Comput. Phys.* **175** (2002) 525-558.
- [14] D. Kuzmin, M. Möller and S. Turek, Multidimensional FEM-FCT schemes for arbitrary time-stepping. Technical report 215: University of Dortmund, 2002. Submitted to *Int. J. Numer Methods Fluids*.
- [15] A. Lapin and A. Lübbert, Numerical simulation of the dynamics of two-phase gas-liquid flows in bubble columns. *Chem. Eng. Sci.* **49** (1994), no. 21, 3661–3674.
- [16] R. Löhner, *Adaptive CFD Techniques*. Wiley, 2001.
- [17] R. Löhner, K. Morgan, J. Peraire and M. Vahdati, Finite element flux-corrected transport (FEM-FCT) for the Euler and Navier-Stokes equations. *Int. J. Numer. Methods Fluids* **7** (1987) 1093–1109.
- [18] P. R. M. Lyra, *Unstructured Grid Adaptive Algorithms for Fluid Dynamics and Heat Conduction*. PhD thesis, University of Wales, Swansea, 1994.
- [19] D. Pflieger, S. Gomes, N. Gilbert and H.-G. Wagner, Hydrodynamic simulations of laboratory scale bubble columns - Fundamental studies of the Eulerian-Eulerian modelling approach. *Chem. Eng. Sci.* **54** (1999) 5091–5098.
- [20] R. Rannacher and S. Turek, A simple nonconforming quadrilateral Stokes element. *Numer. Methods Partial Differ. Equations* **8** (1992), no. 2, 97-111.
- [21] M. P. Schwarz and W. J. Turner, Applicability of the standard $k-\epsilon$ turbulence model to gas-stirred baths. *Appl. Math. Modelling* **12** (1988) 273–279.
- [22] T.K. Sherwood, R.L. Pigford and C.R. Wilke, *Mass Transfer*. McGraw-Hill, New York, 1975.
- [23] A. Sokolichin and G. Eigenberger, Modellierung und effiziente numerische Simulation von Gas-Flüssigkeits-Reaktoren mit Blasenströmungen nach dem Euler-Euler-Konzept. DFG technical report. University of Stuttgart, 1995-1997. Available at <http://pcvt12.verfahrenstechnik.uni-stuttgart.de/alex/icvt2.html>.
- [24] A. Sokolichin, and G. Eigenberger, Applicability of the standard turbulence model to the dynamic simulation of bubble columns: Part I. Detailed numerical simulations. *Chem. Eng. Sci.* **54** (1999) 2273-2284.
- [25] A. Sokolichin, G. Eigenberger, A. Lapin and A. Lübbert, Dynamic numerical simulation of gas-liquid two-phase flows: Euler-Euler versus Euler-Lagrange. *Chem. Eng. Sci.* **52** (1997), no. 4, 611–626.

- [26] S. Turek, On discrete projection methods for the incompressible Navier-Stokes equations: An algorithmical approach. *Comput. Methods Appl. Mech. Eng.* **143** (1997) 271–288.
- [27] S. Turek *et al.*, *FEATFLOW: finite element software for the incompressible Navier-Stokes equations*. User manual, University of Dortmund, 2000. Available at <http://www.featflow.de>.
- [28] S. Turek *et al.*, *FEAT2D/FEAT3D: Finite Element Analysis Tools*. User manual, University of Heidelberg, 1995. Available at <http://www.featflow.de>.
- [29] S. Turek, *Efficient Solvers for Incompressible Flow Problems: An Algorithmic and Computational Approach*, LNCSE 6, Springer, 1999.
- [30] A.M.P. Valli, G.F. Carey and A.L.G.A. Coutinho, Control strategies for timestep selection in simulation of coupled viscous flow and heat transfer. *Commun. Numer. Methods Eng.* **18** (2002), no.2, 131-139.
- [31] D.W. Van Krevelen and P. J. Hoftijzer, Kinetics of gas-liquid reactions. Part I: General Theory. *Rec. Trav. Chim.* **67** (1948) 563–586.
- [32] R. M. Wellek, R. J. Brunson and F. H. Law, *Can. J. Chem. Eng.* **56** (1978) 181.
- [33] S. T. Zalesak, Fully multidimensional flux-corrected transport algorithms for fluids. *J. Comput. Phys.* **31** (1979) 335–362.